Chirality of superfluid ^{3}He-A

P. M. Walmsley and A. I. Golov
School of Physics and Astronomy, The University of Manchester, Manchester M13 9PL, UK
(Dated: September 1, 2012)

We have used torsional oscillators, containing disk-shaped slabs of superfluid ^{3}He-A, to probe the chiral orbital textures created by cooling into the superfluid state while continuously rotating. Comparing the observed flow-driven textural transitions with numerical simulations of possible textures shows that an oriented monodomain texture with $\hat{\mathbf{l}}$ *antiparallel* to the angular velocity $\mathbf{\Omega_0}$ is left behind after stopping rotation. The bias towards a particular chirality, while in the vortex state, is due to the inequivalence of energies of vortices of opposite circulation. When spun-up from rest, the critical velocity for vortex nucleation depends on the sense of rotation, $\hat{\mathbf{\Omega}}$, relative to that of $\hat{\mathbf{l}}$. A different type of vorticity, apparently linked to the slab's rim by a domain wall, appears when $\hat{\mathbf{\Omega}} = \hat{\mathbf{l}}$.

PACS numbers: 67.30.he, 67.30.hb, 47.37+q, 11.30.Rd

Chiral superconductors and superfluids (with spontaneously broken time-reversal and parity symmetry) attract interest because of many properties that depend upon the chosen sense of orbital rotation and of the possibility to have topologically-protected quantum states [1, 2]. To investigate these, a mono-domain texture with a known orientation of the order parameter is required. So far, even in field-cooled samples of chiral p-wave superconductor Sr_2RuO_4, domain sizes not larger than $\sim 1\,\mu$m are reported [3], while the very existence of domain walls separating ground states (vacua) with opposite chiralities was only demonstrated indirectly [4]. Many other desirable proofs of the chiral character of Sr_2RuO_4 (such as the inequivalence of the critical fields and structures of defects for opposite directions of magnetic fields [5, 6]) are yet to be made – and require finding some means of obtaining monodomain samples in the first place.

^{3}He-A is a chiral p-wave superfluid [7] with the unit vector $\hat{\mathbf{l}}$ describing the local direction of the coherent orbital momentum of Cooper pairs. When ^{3}He-A in zero magnetic field is confined between two parallel walls, normal to $\hat{\mathbf{z}}$ and separated by a distance D, $\hat{\mathbf{l}}$ is forced normal to the boundaries, leading to a two-fold degenerate ground state with a uniform $\hat{\mathbf{l}}$ texture (i.e. $\hat{\mathbf{l}} = \pm\hat{\mathbf{z}}$). These chiral textures are the time reversed states of each other. This quasi-2-d ^{3}He-A is analogous to the case of anisotropic Sr_2RuO_4 in which the $\hat{\mathbf{l}}$-vector is aligned with the c-axis. Yet ^{3}He-A differs by the ability of its order parameter to break off the constrain $\hat{\mathbf{l}} \parallel \pm\hat{z}$ at macroscopic lengthscales $\leq D$. While similar to chiral superconductors, ^{3}He-A is free of many problems that plague them: it is free of complicated rotational anisotropy and crystal defects; there is no long-range magnetic interaction between different regions of vorticity and surface currents; its large-core vortices-skyrmions experience no bulk pinning and only very weak pinning by container walls – thus allowing them to be completely removed after stopping rotation.

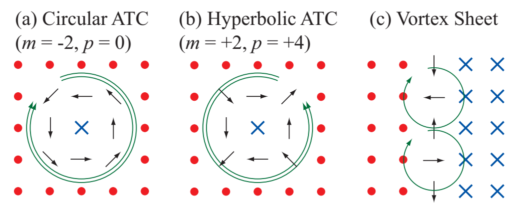

FIG. 1. (Color online). $\hat{\mathbf{l}}$-textures of non-singular vortex states in a mono-domain (a, b) and poly-domain (c) quasi-2d ^{3}He-A. The circles and crosses represent the chiral uniform textures with $\hat{\mathbf{l}} = \hat{\mathbf{z}}$ and $\hat{\mathbf{l}} = -\hat{\mathbf{z}}$ respectively. Black arrows show the orientation of the distorted regions where $\hat{\mathbf{l}} \perp \hat{\mathbf{z}}$. The quanta of velocity circulation are indicated by the green circular arrows.

In the absence of any orientational bias to lift the degeneracy, a transition into the superfluid state produces multiple regions of uniform $\hat{\mathbf{l}}$-texture of both chiral types separated by domain walls; such polydomain textures display reduced critical velocities (identical for rotation in opposite directions) for the Fréedericksz transition and vortex nucleation [8, 10], and also the strong intrinsic pinning of vorticity by the network of domain walls [11]. In this Letter, we demonstrate asymmetry with respect to the sense of rotation in monodomain samples of ^{3}He-A which we succeeded in creating by cooling ^{3}He whilst rotating. The orientation of the obtained $\hat{\mathbf{l}}$-texture was found to be actually *opposite* to the angular velocity of rotation that was producing the bias.

Cooling through the temperature of the second-order phase transition, T_c, whilst rotating at $\hat{\mathbf{\Omega}}_0 = \pm\hat{\mathbf{z}}$ seems to be one way to selectively create the chiral vacuum of the lowest free energy [12]. The Zeeman-like interaction, $\propto -\mathbf{L}_0 \cdot \mathbf{\Omega}_0$, due to the tiny intrinsic orbital momentum $\mathbf{L}_0$ [7] would favor $\hat{\mathbf{l}} \parallel +\mathbf{\Omega}$; however, the effect of quantized vortices should be much greater. As the thermodynamic first critical field is zero in ^{3}He-A, one arrives into the vortex state. Superfluid ^{3}He-A allows a wide variety of vortex types [13, 14] with either singular or continuous cores, and hence several different vortex states. In our conditions (thick slab, zero magnetic field, substantial angular velocities) [15], the continuous vortices-skyrmions of Anderson-Toulouse-Chechetkin (ATC) [13, 16, 17] have the lowest energy. These are metastable $\hat{\mathbf{l}}$-textures with the diameter of the soft core $\sim D$, within which the $\hat{\mathbf{l}}$-vector flips. The circulation of the superfluid velocity round any contour is related to the inhomogeneous $\hat{\mathbf{l}}$-texture within the contour through the Ho theorem [18]. Panels (a) and (b) in Fig. 1 show ATC vortices of opposite senses of circulation embedded in the $\hat{\mathbf{l}} = \hat{\mathbf{z}}$ ground state. They have $m = -2w$ quanta of circulation, $\kappa \equiv h/2m_3$, where the integer w denotes the winding number of the xy component of $\hat{\mathbf{l}}$ inside the core region (taking counterclockwise rotation as positive). The axisymmetric 'circular' vortex (a) with $w = +1$ ($m = -2$) posesses an orbital momentum *antiparallel* with $\hat{\mathbf{l}} = \hat{\mathbf{z}}$, whereas the 'hyperbolic' vortex (b) with $w = -1$ ($m = +2$) has its orbital momentum *parallel* with $\hat{\mathbf{l}} = \hat{\mathbf{z}}$. One can think of their soft cores as of circular domains of the time-reversed state ($\hat{\mathbf{l}} = -\hat{\mathbf{z}}$) surrounded by a domain wall, which is decorated by compact vortex kinks-merons, each with one quantum of circulation. The total circulation is hence $m = -2+p$, where the even integer p gives the number of circulation quanta contributed by kinks: $p = 0$ for circular (a) and $p = +4$ for hyperbolic (b) vortices. An extended domain wall between the degenerate time-reversed ground states, decorated with vortex kinks is generally known as the vortex sheet [14] (Fig. 1(c)).

The free energy in a frame rotating together with the container and viscous normal component is $F = F_0 + \pi R^2 n E_\mathrm{v} - \mathbf{L}\cdot\mathbf{\Omega}$, where F_0 is the free energy in the laboratory frame associated with the underlying global $\hat{\mathbf{l}}$ texture, n is the areal density of vortices, E_v is the energy of a vortex, R is the radius of the container and $\mathbf{L}$ is the total angular momentum. The inequivalence of the two types of ATC vortex suggests that they are capable of providing an orientational bias such that a particular chirality of $\hat{\mathbf{l}}$ is preferred, dependent on which type has the lowest energy E_v. We used the approach of Karimäki and Thuneberg [19] to calculate the free energy for the 2-d ATC vortices. We find that the ratio of energy between the two vortex types is $E_\mathrm{v}(m = -2)/E_\mathrm{v}(m = +2) = 0.89$, thus predicting that the oriented ground state texture with $\hat{\mathbf{l}} = -\hat{\mathbf{\Omega}}_0$ should be favored. Basically, these calculations confirm the expectation that the smoother $\hat{\mathbf{l}}$-texture of the soft core of the circular vortex ($p = 0$) results in a lower vortex energy than the kinked core of the hyperbolic vortex ($p = 4$). As kinks generally add energy, the vortex with fewer kinks (smaller $|p|$) should have the lowest energy. The formula $m = -2 + p$ then suggests the equilibrium vortex state is that with $p = 0$, i. e. $m = -2$.

We investigated textures, using the torsional oscillator (TO) technique, in ^{3}He-A inside two different disk-shaped cavities, both with radius $R = 5.0$ mm, but with thicknesses $D \approx 0.26$ and 0.41 mm. In this geometry,

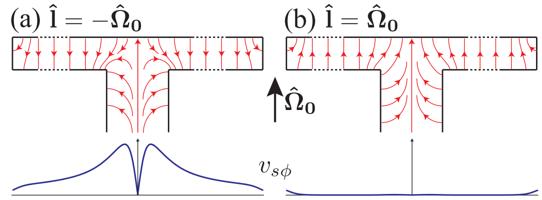

FIG. 2. (Color online). The two possible textures (mainly the distorted textures at the rim and at the fill line in the centre of our disk-shaped cavities are shown, while the extended uniform textures, $\hat{\mathbf{l}} = \pm\hat{\mathbf{z}}$, in between are skipped for clarity) and their associated azimuthal component of superflow, $v_{s\phi}$ (from Eq. 1). $\hat{\mathbf{l}} = -\hat{\mathbf{\Omega}}_\mathbf{0}$ (left, a) and $\hat{\mathbf{l}} = \hat{\mathbf{\Omega}}_\mathbf{0}$ (right, b).

there are two additional factors that affect the texture: the edges of the disk and the filling line (of radius 0.4 mm) that arrives via the torsion stem into the disk on its axis. While the texture inside the fill line has negligible effect on the TO properties, the way it merges with the texture in the slab is important because (as was indeed the case) it might possess an additional two-quantum vortex. The TO resonance frequency and width are sensitive to counterflow velocity, particularly near the rim of the disk, through the changes in the anisotropic density and viscosity of the normal component resulting from flow-induced azimuthal tilting of $\hat{\mathbf{l}}$. The TOs were mounted on a rotating nuclear demagnetization cryostat with the disk's axes aligned with the rotation axis of the cryostat ($\hat{z} \parallel \Omega$). All experiments were at 29.3 bar pressure and with temperatures in the range 2–2.5 mK. The motion of the TOs was driven and detected capacitively at a frequency close to the resonant frequencies of ν_R= 627 and 674 Hz and the full width at half maximum (bandwidth) was ν_B=0.12 Hz and 0.25 Hz for the thin and thick slabs respectively. The viscous penetration depth was $\sim D$; hence, both ν_R and ν_B showed a similar response so we used whichever had the better signal to noise ratio.

To create oriented textures, we cooled through $T_\mathrm{c} = 2.5$ mK at a rate of $\sim 1\,\mu$K min^{-1} whilst rotating the cryostat at $\mathbf{\Omega_0} = \pm 0.42\hat{\mathbf{z}}$ rad s^{-1}. The magnitude of $\mathbf{\Omega_0}$ was chosen so that the texture in the fill line was the Mermin-Ho type with $1\kappa\hat{\mathbf{\Omega}}_\mathbf{0}$ of circulation and had $\hat{\mathbf{l}} = \hat{\mathbf{\Omega}}_\mathbf{0}$ on axis. It also ensured that the distance between vortices in the slab, $\simeq (\kappa/\Omega_0)^{1/2} = 0.4$ mm, is sufficiently large that their soft cores of radius $\simeq D/2$ are well-separated. We thus can treat the texture in the slab as an array of ATC vortices embedded in a uniform oriented texture. After cooling well below T_c, the rotation was stopped, and the majority of vortices left the slab. The cryostat was then rotated gently in the opposite direction with $\mathbf{\Omega} = -0.01\hat{\mathbf{\Omega}}_\mathbf{0}$ rad/s to remove any (typically 3–8) weakly pinned vortices [10].

The two types of oriented monodomain texture $\hat{\mathbf{l}} = \pm\hat{\mathbf{\Omega}}_\mathbf{0}$, possible in our geometry, are shown in Fig. 2. If $\hat{\mathbf{l}} = \hat{\mathbf{\Omega}}_\mathbf{0}$ then the texture is the Mermin-Ho type and

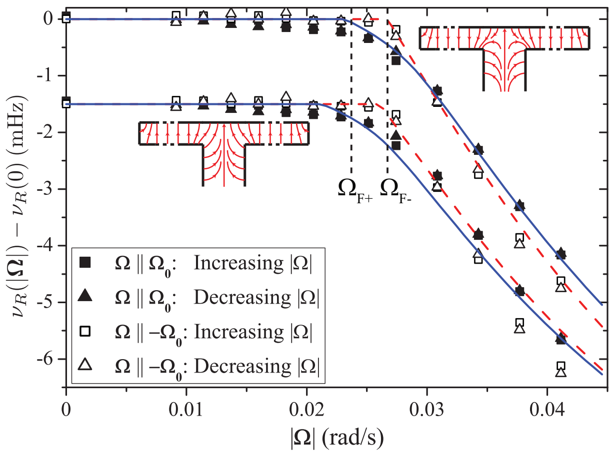

FIG. 3. (Color online). The shift in $\nu_{\rm R}(\Omega)$ for the $D = 0.26\,$mm slab due to the flow-induced Fréedericksz transition for both directions of rotation. The lines (solid blue: $\mathbf{\Omega} \parallel -\hat{\mathbf{l}}$, dashed red: $\mathbf{\Omega} \parallel \hat{\mathbf{l}}$) are calculated using Eqn. 2 for the two possible types of oriented textures (top: $\hat{\mathbf{l}} = -\hat{\mathbf{\Omega}}_{\mathbf{0}}$ as on Fig. 2(a); bottom (shifted by -1.5 mHz for clarity): $\hat{\mathbf{l}} = \hat{\mathbf{\Omega}}_{\mathbf{0}}$ as on Fig. 2(b)). They are compared with the typical experimental data, $\mathbf{\Omega} \parallel \pm\mathbf{\Omega_0}$ (same data points are also repeated shifted by -1.5 mHz). $T = 0.9T_{\rm c}$ and $C = -18\,$mHz.

there will be $+1\kappa\hat{\mathbf{\Omega}}_{\mathbf{0}}$ of circulation due to the bending of $\hat{\mathbf{l}}$ within a distance $\simeq D$ from the outer perimeter of the slab (Fig. 2(b)). Alternatively, if $\hat{\mathbf{l}} = -\hat{\mathbf{\Omega}}_{\mathbf{0}}$ then the orientation of the texture in the slab is opposite to that in the centre of the fill line, and "stitching" these textures together will result in a vortex with $+2\kappa\hat{\mathbf{\Omega}}_{\mathbf{0}}$ of circulation trapped in the centre. There will also be $-1\kappa\hat{\mathbf{\Omega}}_{\mathbf{0}}$ contribution that again arises from the bending of $\hat{\mathbf{l}}$ at the perimeter (Fig. 2(a)). In both of these cases, the azimuthal component of superflow is given by

$$v_{s\phi} = \frac{(1-l_z)\kappa}{2\pi r}. \qquad (1)$$

To figure out which of these textures was formed, we rotated the cryostat at $\Omega > \Omega_{\rm F} \simeq v_{\rm F}/R$ to induce the flow-driven Fréedericksz transition [8] while tracking changes in $\nu_{\rm R}$ and $\nu_{\rm B}$. This was done for both directions of rotation ($\mathbf{\Omega} \parallel \pm\mathbf{\Omega_0}$) but with care not to nucleate vortices. The observed shifts, $\Delta\nu_{\rm R}(\mathbf{\Omega})$ (shown in Fig. 3) were reversible with increasing/decreasing Ω. There are reproducible differences for opposite senses of rotation that have been observed in both slabs investigated: for ($\mathbf{\Omega} \parallel \mathbf{\Omega_0}$), the onset of the Fréedericksz transition occurs at a lower $\Omega_{\rm F+}$, and then the TO frequency $\nu_{\rm R}(|\Omega|)$ drops with a shallower slope compared to rotation in the opposite direction (where the transition is noticeably sharper and at a larger $\Omega_{\rm F-}$) [20] – so that two $\nu_{\rm R}(|\Omega|)$ quickly change hands before becoming nearly parallel.

To elucidate the $\hat{\mathbf{l}}$ texture obtained in the experiment, we have numerically calculated $\hat{\mathbf{l}}(r, z, \mathbf{\Omega})$ in the slab by minimizing the free energy [21]. The calculated textures were converted into a frequency shift using

$$\nu_R(\mathbf{\Omega}) - \nu_R(0) = \frac{2C}{\pi D R^4}\int r^2 l_\phi(r, z, \mathbf{\Omega})\,{\rm d}V, \qquad (2)$$

where $C \propto \rho_s(T)$ is a fitting parameter to provide the correct frequency scaling. In addition, the effective D was increased from 0.26 to 0.28 mm so that the calculated values of $\Omega_{\rm F}$ coincided with the measurements. The calculated frequency shifts are compared to the experimental data in Fig. 3. Clearly the oriented texture with $\hat{\mathbf{l}} = -\hat{\mathbf{\Omega}}_{\mathbf{0}}$ best reproduces all observed differences in the response of the torsional oscillator for the different directions of rotation. The observed asymmetry results from the combined effect of a trapped double-quantum vortex and the coupling between the applied flow and the non-uniform texture at the perimeter of the slab [21]. We thus confirm our theoretical calculations that $\hat{\mathbf{l}} = -\hat{\mathbf{\Omega}}_0$ is formed by our technique.

Further evidence for the presence of an oriented texture can be seen in the difference between the critical angular velocities for vortex nucleation, Ω_c, for $\mathbf{\Omega} \parallel \pm\mathbf{\Omega_0}$, and in the case of the thicker slab the subsequent motion of vorticity is entirely different for rotation with $\mathbf{\Omega} \parallel -\mathbf{\Omega_0}$. When an oriented texture is rotated with $\mathbf{\Omega}||\mathbf{\Omega}_0$, circular ATC vortices will be nucleated near the outer rim and then move towards the centre of the disk, forming a vortex cluster, such that $v(R) = v_{\rm c} = \Omega_{\rm c}R$. Upon slowing down, the vortex cluster expands and vortices are able to leave, so a uniform equilibrium distribution of vortices $n = \Omega/\kappa$ is maintained. These rotations with $\mathbf{\Omega} \parallel \mathbf{\Omega_0}$ (which introduced up to $\simeq 500$ ATC vortices) always left behind the original defect-free oriented texture after stopping rotation. The "Ω-loops" (like magnetization loops for type-II superconductors) thus show hysteresis in the measured TO properties associated with vortex nucleation at finite $v_{\rm c}$ [10] (see Fig. 4(d)). For $D = 0.26\,$mm (0.41 mm) we found $v_{\rm c+} \approx 0.6\,{\rm mm\,s^{-1}}$ ($0.3\,{\rm mm\,s^{-1}}$). We thus interpret $v_{\rm c}(D)$ that decreases with increasing D as $v_{\rm c} \approx 4v_{\rm F} \propto D^{-1}$ as the critical velocity for vortex nucleation near the disks edge corners where the $\hat{\mathbf{l}}$-texture is severely distorted due to the boundary conditions at the walls [22]. These critical velocities are consistent with vortices having *continuous* cores, for which $v_{\rm c} \sim \kappa/D \sim 0.2\,{\rm mm\,s^{-1}}$ [10], and not with those having *singular* cores with $v_{\rm c} \sim \kappa/\xi_{\rm d} \sim 70\,{\rm mm\,s^{-1}}$ [24] ($\xi_{\rm d} \approx 10\,\mu$m is the dipole length above which the spin and orbital degrees of freedom are coupled).

Fast rotation with $\mathbf{\Omega} \parallel -\mathbf{\Omega_0}$ is expected to nucleate hyperbolic ($m = +2, p = +4$) ATC vortices, which when far from the rim will behave the same way as the previously discussed circular ATC vortices. This appears to be the case for the 0.26 mm slab, where we observe similar Ω-loops albeit with reduced $v_{\rm c-} \simeq 0.4$ mm/s. The oriented texture still remained after rotation is stopped. However, the behavior for the 0.41 mm slab is very different: even though there are clear evidences of vortex nucleation

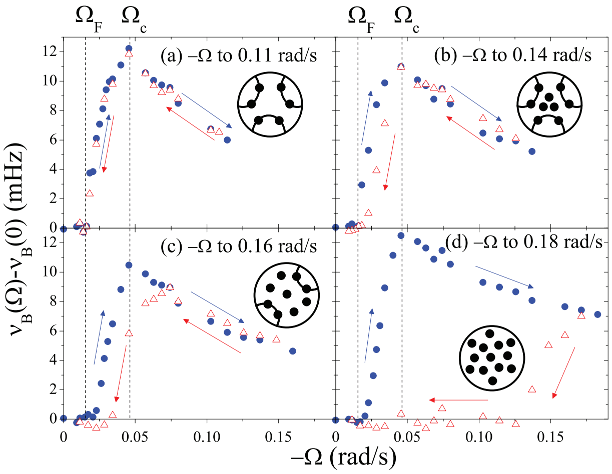

FIG. 4. (Color online). $\Delta\nu_B$ in the 0.41 mm thick slab for a series of rotation sweeps with $\mathbf{\Omega} \parallel -\mathbf{\Omega_0}$. Solid (open) symbols are for increasing (decreasing) $|\Omega|$. The cartoons indicate how some vorticity is bound to the rim of the container.

above $v_{\rm c-} \simeq 0.25\,{\rm mm/s}$ ($\Omega_{\rm c-} \simeq 0.05\,{\rm rad/s}$), the Ω-loops are still non-hysteretic! Only above $\Omega \simeq 0.14\,{\rm rad/s}$ does the hysteresis gradually set in (indicating that the nucleated vortices stay in the central cluster). Fig. 4 shows changes in ν_B for a series of rotation sweeps to progressively higher Ω. $\nu_{\rm B}$ increases when $\Omega > \Omega_{\rm F-}$ but then begins to decrease when $\Omega_{\rm c-}$ ($v_{\rm c-} \simeq 0.25\,{\rm mm\,s^{-1}}$) is reached due to the creation of vorticity ($v_{\rm c-} \propto D^{-1}$ for this direction of rotation as well). If the rotation was slowed after reaching a maximum of 0.11 rad/s as shown in Fig. 4(a) (corresponding to introducing $\simeq 140\kappa$) then there is no hysteresis at all. If the maximum angular velocity is now increased to 0.14 rad/s (Fig. 4(b)) then there is some slight hysteresis during the final part of the deceleration. The next rotation (Fig. 4(c)) has a slightly higher $\Omega_{\rm F-}$ consistent with $\simeq 20\kappa$ being trapped from the previous rotation sweep. Unlike vortices introduced by rotations in the original direction, $\mathbf{\Omega}||\mathbf{\Omega}_0$, this vorticity is now strongly pinned [11], and cannot be removed by gentle rotation in the opposite direction. It also seems that defects had been irreversibly introduced into the texture as the behavior for small Ω ($\Omega_{\rm F-} < \Omega < \Omega_{\rm c-}$) was changed and no longer corresponded to the ones shown in Fig. 3. Further rotation to higher angular velocities introduces more hysteresis (Fig. 4(c&d)). The fact that no hysteresis is seen just above $\Omega_{\rm c-}$ means that vortices can be reversibly removed upon (even small) deceleration, which is extraordinary!

We suggest a speculative scenario that the non-hysteretic vortex behavior results from vorticity that is bound to the disk's rim. This could occur when a crescent-shaped domain of $\hat{\mathbf{l}} = \hat{\mathbf{\Omega}}_\mathbf{0}$ is formed. Its domain wall will have a reduced critical velocity for the nucleation of vortex kinks [23] and can either become decorated with four vortex kinks and detach from the wall forming an individual $m = +2, p = +4$ ATC vortex which will migrate towards the centre of the disk (as apparently happens in the thinner slab), or it can stretch and become further decorated with vortex kinks forming a vortex sheet (Fig. 1(c)). The ends of the vortex sheet will remain attached to the rim while the vortex kinks will be attracted towards the centre but this will be resisted by the tension of the domain wall. The non-hysteretic behavior probably results from the nucleation of multiple vortex sheets, such a vortex configuration shows very little hysteresis in bulk ^{3}He-A [25]. The sheets are able to shrink and disappear upon deceleration, until a second critical velocity ($\simeq 0.14$ rad/s) is reached when certain domain walls and kinks remain after rotation is stopped, perhaps due to pinning. Further rotations then show more hysteresis as the kinks are no longer bound to the rim and move towards the centre of the disk. The fact that, following the rotation, at Ω well-above $\Omega_{\rm c-}$, in the direction opposite to that of $\mathbf{\Omega}_0$ the initially monodomain texture is permanently ruined (as judged by the Fréedericksz transition) also tells that domain walls have been introduced along with vortex nucleation. This seems to be a natural process of gradual replacement of the metastable vortex state with hyperbolic vortices in $\hat{\mathbf{l}}||\mathbf{\Omega}$ texture by that with circular vortices in $\hat{\mathbf{l}}|| - \mathbf{\Omega}$ texture.

By breaking the time-reversal symmetry of the two competing ground states of chiral ^{3}He-A by rotation at $\mathbf{\Omega}_0$, we have created large monodomain samples of ^{3}He-A in a slab geometry and, for the first time, determined their orientation $\hat{\mathbf{l}}$ as a function of the bias: $\hat{\mathbf{l}}||-\mathbf{\Omega}_0$. This orientation is opposite to that expected from the interaction with the intrinsic orbital moment, but is due to the differences in the structures of vortex-skyrmions with opposite senses of circulation. It is hence the -2 in the formula $m = -2 + p$ that explains that the lower-energy vortices with circular core ($p = 0$) are embedded into the $\hat{\mathbf{l}}$-texture oriented *opposite* to the sense of initial rotation. In chiral superconductors, thanks to the inequivalence of energies of vortices with opposite senses of circulation [6], it might also be possible to create monodomain $\hat{\mathbf{l}}$-textures by a similar technique (i. e. slow field-cooling into the vortex state in a substantial magnetic field up to $H \sim H_{\rm c2}$); this will result in $\hat{\mathbf{l}}||-\mathbf{H}$ orientation which is opposite to the one favored by field-cooling experiments with small fields $H \ll H_{\rm c1}$ [3].

We acknowledge discussions with H. E. Hall and the contribution of S. May in the construction of the experiment. Support provided by EPSRC under GR/N35113, EP/E001009 and through the award of a Career Acceleration Fellowship to PMW (EP/I003738).

[1] A. P. Mackenzie and Y. Maeno, Rev. Mod. Phys. **75**, 657 (2003).

[2] H. Nobukane et al., Phys. Rev. B **83**, 144502 (2011).

[3] F. Kidwingira et al., arxiv:1002.1430v1 (2010).

[4] F. Kidwingira et al., Science **314**, 1267 (2006).

[5] T. A. Tokuyasu, D. W. Hess, and J. A. Sauls, Phys. Rev. B **41** 8891 (1990).

[6] J. A. Sauls and M. Eschrig, New J. Phys. **11**, 075008 (2009).

[7] D. Vollhardt and P. Wölfle, *The Superfluid Phases of Helium 3* (Taylor & Francis, London, 1990).

[8] A counterflow ($\mathbf{v} \equiv \mathbf{v_n} - \mathbf{v_s}$) applied parallel to the boundaries favors $\hat{\mathbf{l}}$ to be aligned with $\mathbf{v}$. The uniform texture persists until the critical velocity $v_F \simeq \sqrt{5}\kappa/4D$ is reached when $\hat{\mathbf{l}}$ begins to tip in the middle ($z = 0$) in order to align with the flow [9]. This flow-driven Fréedericksz transitions has been observed experimentally [10] and forms the basis of our characterization technique.

[9] A. L. Fetter, Phys. Rev. B **14**, 2801 (1976).

[10] P. M. Walmsley, D. J. Cousins and A. I. Golov, Phys. Rev. Lett. **91**, 225301 (2003)

[11] P. M. Walmsley, I. J. White and A. I. Golov, Phys. Rev. Lett. **93**, 195301 (2004)..

[12] T. D. C. Bevan et al., J. Low Temp. Phys. **109**, 423 (1997).

[13] M. M. Salomaa and G. E. Volovik, Rev. Mod. Phys. **59**, 533 (1987).

[14] Ü. Parts *et al.*, Phys. Rev. Lett. **75**, 3320 (1995).

[15] C. R. Hu, T. E. Ham, W. M. Saslow, J. Low Temp. Phys. **32**, 301 (1978).

[16] P. W. Anderson and G. Toulouse, Phys. Rev. Lett. **38**, 508 (1977).

[17] V. R. Chechetkin, Sov. Phys. JETP, **44**, 766 (1976).

[18] T.-L. Ho, Phys. Rev. B **18** 1144 (1978).

[19] J. M. Karimäki and E. V. Thuneberg, Phys. Rev. B **60**, 15290 (1999).

[20] We ascribe + (−) index to the critical velocities for rotation in the same (opposite) direction as that of $\mathbf{\Omega}_0$ at which the texture was created.

[21] See supplementary material for details of the texture calculation.

[22] This interpretation of the nature of v_c differs from that given in [10] in which on the basis of the proximity of $v_{c+} = 0.6\,\mathrm{mm\,s^{-1}}$ (for the 0.26 mm slab) with the $v_{c0} \simeq 1\,\mathrm{mm\,s^{-1}}$ due to the bulk dipole-unlocking instability when $\hat{\mathbf{l}} \parallel \pm\mathbf{v}$ [23].

[23] J. Kopu, R. Hänninen and E. V. Thuneberg, Phys. Rev. B **62**, 12374 (2000).

[24] V. M. H. Ruutu *et al.*, Phys. Rev. Lett. **79**, 5058 (1997).

[25] V. B. Eltsov *et al.*, Phys. Rev. Lett. **88**, 065301 (2002).